

Uptake of Toxic Metal Ions from Water by Naked and Monolayer Protected Silver Nanoparticles: An X-ray Photoelectron Spectroscopic Investigation

M. S. Bootharaju and T. Pradeep*

DST Unit on Nanoscience (DST UNS), Department of Chemistry and Sophisticated Analytical Instrument Facility, Indian Institute of Technology Madras, Chennai 600 036, India

Received: March 5, 2010; Revised Manuscript Received: April 7, 2010

We have studied the chemical interaction of heavy metal ions such as Hg(II), Hg(I), Pb(II), and Cd(II) of various concentrations with naked and protected silver nanoparticles (Ag@citrate and Ag@MSA, respectively, where MSA is mercaptosuccinic acid). The particles were of 30 and 8 nm diameter, respectively. We observed that the metal ions interact with both the core of the nanoparticles and the functional groups of the capping agents. We study the effects of interaction using spectroscopic and microscopic techniques such as ultraviolet–visible spectroscopy (UV–vis), Fourier transform infrared spectroscopy (FTIR), X-ray diffraction (XRD), scanning electron microscopy (SEM), transmission electron microscopy (TEM), dynamic light scattering (DLS), and in detail by X-ray photoelectron spectroscopy (XPS). The Hg(II) and Hg(I) ions were reduced to metallic mercury by both of the nanoparticles, because of the feasibility of the redox reaction, whereas no reduction was observed for Cd(II) and Pb(II). The reduction of Hg(I) and Hg(II) ions was due to electrons supplied by the core silver atoms of the nanoparticles, at lower metal ion concentrations. At higher concentrations, the metal ions were chemically bonded to the carboxylate groups of the citrate and MSA. These heavy metal ions form stable sulfides. The presence of different sulfur species, such as oxidized sulfur, disulfides, and metal sulfides, was confirmed by XPS.

Introduction

Heavy metal contamination of groundwater resources is one of the major threats facing mankind. The release of mercury into water caused devastating public health hazards such as the Minamata^{1–3} disease. Solvated mercuric ion is stable and is carcinogenic with high cellular toxicity.⁴ The United States Environmental Protection Agency has set a maximum limit of 2 ppb for mercuric ion in drinking water.⁵ Mercury contamination has been reported in several parts of the world including Asian countries (India, China, Japan, Kazakhstan, Korea Democratic Republic, Israel, etc.),^{6a} Canada, USA, Germany, Great Britain, Australia, and so forth.^{6b} Major industrial segments which cause such release are pharmaceuticals, paper industries, chemical manufacturing, coal burning, gold–silver mining, mercury mining, biomass burning, and natural events such as volcanic eruptions, forest fires, and so forth.⁷ An affordable solution for mercury decontamination is still not available. Nanomaterial-based adsorbents for Hg(II) uptake are indeed a worthwhile possibility. Gold nanoparticles loaded on alumina (Al₂O₃) have been shown to remove Hg(II) after its reduction to Hg(0), followed by amalgamation.⁸ An uptake capacity of 4.065 g per 1 g of gold nanoparticle has been demonstrated. However, the uptake was significantly reduced when Hg(II) was used directly. Several other remedial measures including nano zerovalent iron (nzvi) has been proposed.⁹ Gold nanorod-based determination of Hg(II) in water has been reported up to parts per trillion.¹⁰

Noble metal nanoparticles have emerged as potential materials for water purification in the recent past.¹¹ Catalytic decomposition of halogenated pesticides,¹² efficient uptake of several molecules, antibacterial properties,¹³ absence of toxicity to

humans, excellent stabilization on inert substrates such as alumina, and aqueous synthetic routes for large-scale production with minimal environmental impact are all important benefits for these systems. From these perspectives, noble metal nanoparticle-based adsorbent systems are practical solutions for drinking water purification.¹⁴

Although several studies have investigated gold from the perspective of heavy metal remediation, investigations to such depth have not happened with silver. In this report, we study the interaction of several toxic metal ions on two distinct silver nanoparticle systems, namely, Ag@citrate and Ag@MSA (MSA = mercaptosuccinic acid). While the former nanoparticle system is a charge-stabilized colloid of large polydispersity, the latter is more monodispersed with reduced particle size. We investigate the nature of interaction between the metal ions and the nanoparticles. The roles of metal nanoparticle core and monolayer of the capping agent in the metal ion removal are investigated in detail. Distinctly different chemical species have been identified on the surfaces. Both of these nanoparticles can be stabilized on suitable inert substrates and can be used for applications.

Experimental Section

Materials. Silver nitrate (CDH, India), trisodium citrate (TSC, Qualigens), MSA, methanol (SRL Chemical Co. Ltd., India), sodium borohydride (Sigma Aldrich), mercuric acetate (Ranbaxy), mercurous nitrate (Ranbaxy), lead acetate (Rankem), and cadmium acetate (Merck) were purchased from various laboratories (mentioned in brackets) and used as such without further purification.

Synthesis of Ag@citrate Nanoparticles. The Ag@citrate nanoparticles were prepared according to the reported protocol.¹⁵ In this method, to a boiling 500 mL silver nitrate (1 mM)

* To whom correspondence should be addressed. E-mail: pradeep@iitm.ac.in.

solution, 20 mL of 1 wt % TSC was added, and heating was continued further for few minutes. The solution turned light yellow in color, indicating the formation of nanoparticles. The suspension was cooled in an ice bath to allow the growth of nanoparticles. Later, the solution was centrifuged, and the precipitate was washed with distilled water to remove excess citrate. Finally, the same volume of distilled water was added to the wet nanoparticles, which were used for the treatment of metal ions.

Synthesis of Ag@MSA Nanoparticles. Ag@MSA nanoparticles were prepared as per the published literature.¹⁶ About 448.9 mg of MSA was dissolved in 100 mL of methanol with stirring, under ice-cold conditions. To this, AgNO₃ solution (85 mg of AgNO₃ in 1.7 mL of distilled water) was added. Then 25 mL of 0.2 M sodium borohydride solution was added dropwise, and stirring was continued for one hour. The precipitate of nanoparticles was centrifuged and washed several times with methanol to remove excess sodium borohydride and MSA. Finally, the solvent methanol was evaporated with a rotavapor to get nanoparticles in the solid state. These nanoparticles are dispersible in water, because the carboxylic acid groups of the nanoparticles are hydrogen bonded with water.^{17–19}

To treat silver nanoparticles with metal ions, we made 50 mL of Ag@citrate nanoparticles containing the required concentration of metal ions (e.g., for 50 mL of 100 ppm Hg(II) solution, we mixed 25 mL of 200 ppm Hg(II) solution and 25 mL of Ag@citrate nanoparticles). Different concentrations such as 10, 50, and 100 ppm were used. The quantity of Ag@citrate was maintained constant (25 mL) in all of the reactions. In the Ag@MSA case, up to 50 mL of a particular concentration metal ion and 8 mg of Ag@MSA nanoparticles were added. All of the reactions were performed for 24 h, at room temperature. Subsequently, the solutions were subjected to analyses.

Ag metallic particles were made by the NaBH₄ reduction of AgNO₃. Typically to a 25 mL, 0.2 M solution of AgNO₃, 25 mL of 0.2 M NaBH₄ was added and stirred vigorously to get a black powder of Ag. This was washed and used for uptake experiments.

Instrumentation. UV–vis spectra were measured with a PerkinElmer Lambda 25 instrument in the range of 200 to 1100 nm. The Fourier transform infrared (FTIR) spectra were measured with a PerkinElmer Spectrum One instrument. KBr crystals were used as the matrix for preparing the samples. High-resolution transmission electron microscopy (HRTEM) of the samples was carried out using a JEOL 3010 instrument with a UHR pole piece. TEM specimens were prepared by drop-casting one or two drops of aqueous solution to carbon-coated copper grids and allowed to dry at room temperature overnight. All measurements were done at 200 kV to minimize the damage of the sample. Scanning electron microscopy (SEM) images and energy dispersive analysis of X-rays (EDAX) studies were done using a FEI QUANTA-200 SEM. For SEM measurements, samples were drop-casted on an indium tin oxide (ITO) coated conducting glass and dried. X-ray diffraction (XRD) data were collected with a Shimadzu XD-D1 diffractometer using Cu K α radiation ($\lambda = 1.54 \text{ \AA}$) radiation. The samples were scanned in the 2θ range of 10 to 90°. All of the peaks were assigned and compared with the database published by the Joint Committee on Powder Diffraction Standards (JCPDS). Dynamic light scattering (DLS) and ζ potential measurements were performed with Zetasizer 3000HSA (Malvern Instruments, UK).

X-ray photoelectron spectroscopy (XPS) measurements were conducted using an Omicron ESCA Probe spectrometer with unmonochromatized Mg K α X-rays (energy = 1253.6 eV). The

X-ray power applied was 300 W. The pass energy was 50 eV for survey scans and 20 eV for specific regions. Sample solution was spotted on a molybdenum sample plate and dried in vacuum. Spectra in the required binding energy range were collected, and an average was taken. Each spectrum was scanned eight times (except survey scan, which was scanned only once). While taking the spectra, the scan step per second was maintained the same for all of the narrow scans. Beam-induced damage of the sample was reduced by adjusting the X-ray flux. The base pressure of the instrument was 5.0×10^{-10} mB. The binding energy was calibrated with respect to the adventitious C 1s feature at 285.0 eV. Most of the spectra were deconvoluted to their component peaks, using the software CASA-XPS. We arrived at the best possible fits assuming full width at half-maximum (fwhm) to be the same for all of the components of the given peaks, area ratios of the components to be constant (for the p orbital 2:1, the d orbital 1.5:1, and the f orbital 1.33:1), and spin–orbit splitting to be the same (Hg 4f, 4.0 eV; Ag 3d, 6.0 eV; S 2p, 1.2 eV; Cd 3d, 6.7 eV; Pb 4f, 4.8 eV).

Results and Discussion

Characterization of Nanoparticles. As we^{12,13} and others^{17–19} have studied Ag@citrate and Ag@MSA nanoparticles in significant detail before, we provide only essential aspects here.

The Ag@citrate and Ag@MSA nanoparticles showed UV–vis absorption peaks at 411 and 391 nm, respectively, as shown in Figure S1 (Supporting Information, SI). These peaks are due to surface plasmon resonance of metallic silver nanoparticles. The TEM images of Ag@citrate and Ag@MSA nanoparticles are shown as insets in Figure S1. The sizes of Ag@citrate and Ag@MSA nanoparticles were 15–40 and 5–10 nm, respectively. The particles show high polydispersity, characteristic of silver particles. The IR spectra of Ag@citrate and Ag@MSA nanoparticles are shown in Figure S2A (SI). Ag@citrate showed an IR peak at 3432 cm⁻¹ which may be due to O–H stretching of citrate. The other prominent peak at 1597 cm⁻¹ may be due to asymmetric stretching of –COO⁻. The peaks at 2918 and 2856 cm⁻¹ are assigned to the –CH₂– stretching vibrations. A strong peak at 1384 cm⁻¹ is due to the –CH₂– scissoring mode. The peaks at 1061 cm⁻¹ (C–C stretching), 1162 cm⁻¹ (out of phase (CCO)_{alcohol} stretching), and 669 cm⁻¹ (–COO⁻ bending mode) can be assigned to the various molecular modes.^{20,21} In the IR spectrum of Ag@MSA nanoparticles, the absence of a peak around 2548 cm⁻¹ indicates that the capping of the nanoparticles occurred through the sulfur atom, losing the thiolate hydrogen.²² A peak at 3412 cm⁻¹ is due to O–H stretching from bound water.¹⁸ The peaks at 2923 and 2851 cm⁻¹ can be attributed to –CH₂– stretching. The peaks at 1634 and 1572 cm⁻¹ are due to asymmetric stretching of –COO⁻, and the peak at 1398 cm⁻¹ is due to symmetric stretching of –COO⁻. The 1385 cm⁻¹ peak is due to the –CH₂– scissoring mode. The peak at 1060 cm⁻¹ is assigned to the C–C stretching mode, and that at 663 cm⁻¹ is due to the –COO⁻ bending mode.

The XRD spectra of Ag@citrate and Ag@MSA nanoparticles showed characteristic diffractions from (111), (200), (220), (311), and (222) planes as shown in Figure S2B (SI). All of the peaks are indexed and compared with the JCPDS data file (4-783) indicating the presence of metallic silver in a *fcc* lattice. From the TEM image of single Ag@citrate and Ag@MSA nanoparticles, the lattice parameter observed was 0.234 nm, which may be indexed to the (111) crystal facet of *fcc* silver.^{23,24} In Ag@citrate nanoparticles the XRD peaks were sharp, whereas in the Ag@MSA nanoparticles, XRD peaks were broad and less intense, because of their small size.

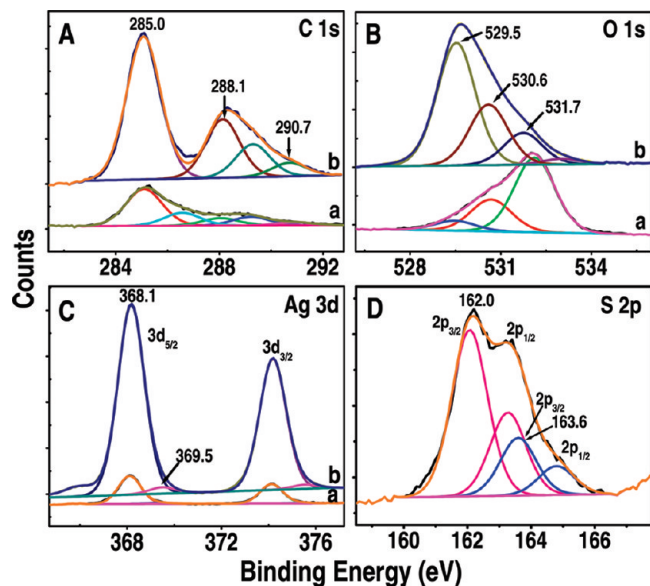


Figure 1. Spectra in the (A) C 1s, (B) O 1s, and (C) Ag 3d of Ag@citrate and Ag@MSA and (D) S 2p region of Ag@MSA. Traces a and b in A, B, and C are due to Ag@citrate and Ag@MSA, respectively.

The XPS survey spectra of Ag@citrate and Ag@MSA nanoparticles are shown in Figure S3 (SI), and the specific regions are expanded in Figure 1. The C 1s binding energies at 288.1 (± 0.2), 289.3 (± 0.2), and 290.7 (± 0.2) eV in both nanoparticles suggest the presence of carboxylate groups.^{25,26} These three positions indicate the presence of carboxylate groups in three different chemical environments such as in intra- and intermolecular hydrogen bonded states¹⁷ and bonding to Ag atoms.²⁶ The peak at 529.5 (± 0.3) eV in Figure 1B corresponds to oxides of silver;²⁵ 530.6 (± 0.3) eV may be due to the hydroxyl group of the citrate, 532.0 (± 0.3) eV is assigned to carboxylate oxygens attached to silver, and 533.0 (± 0.3) eV is assigned to adsorbed water molecules.²¹ The Ag 3d_{5/2} peaks at 368.2 and 368.1 eV, in Figure 1C (traces a and b), correspond to metallic silver (Ag(0)), which matches with the literature.^{27,28} Another weak peak of Ag 3d_{5/2} at 369.5 eV in both Ag@citrate and Ag@MSA may be due to the bonding between silver and the stabilizing agent.^{28,29} The presence of S 2p_{3/2} at 162.0 eV in Figure 1D suggests that the capping agent is chemically bonded to silver nanoparticles in the form of thiolates.³⁰ The S 2p_{3/2} state at 163.6 eV due to the X-ray beam induced damage of thiolates. It is clear from the spectra that X-ray induced damage of the thiolate is insignificant here, as it would have otherwise produced sulfate and sulfite features at higher binding energies.³¹

Treatment of Ag@citrate Nanoparticles with Hg(II). The UV–vis spectra of the nanoparticles upon reaction with Hg(II) solutions showed broad peaks which shifted to higher wavelength, although without any systematic trend, as shown in Figure S4 (SI). The solutions of 0.05, 0.1, 10, 50, and 100 ppm showed the UV–vis peaks at 422, 422, 466, 451, and 451 nm, respectively. This indicates that, after reacting with mercuric ions, agglomeration of nanoparticles occurred.³² This is supported by DLS measurements (see below). The IR spectra of the reaction mixtures (after drying to powder) showed a shift in the carboxylate peak, as shown in Figure S5. The shifts of carboxylate peaks in the Ag@citrate nanoparticle environment is much smaller than in bulk Hg-citrate. The IR spectrum of Hg-citrate is shown in Figure S6 (SI). The strong peaks at 1570 and 1347 cm^{-1} are due to the carboxylate ion as mentioned before. The intensity of the 1631 cm^{-1} feature is less, which is

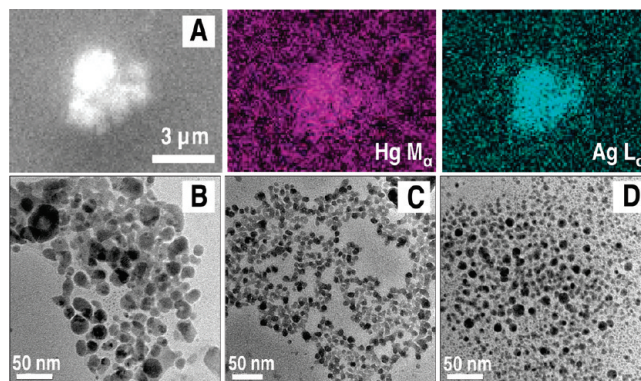


Figure 2. Elemental mapping of aggregated Ag@citrate nanoparticles (A), formed after treating with 100 ppm Hg(II) solution taken in SEM. Scale in Hg M α and Ag L α elemental maps is the same as in A. TEM images of Ag@citrate nanoparticles after treating with 0.1, 10, and 100 ppm (B, C, and D) Hg(II) solutions, after 24 h.

due to O–H bending. The peak at 1597 cm^{-1} in Ag@citrate got shifted to 1587, 1580, and 1582 cm^{-1} in 10, 50, and 100 ppm residues, respectively (Figure S5). These systematic shifts may be due to the increasing interaction between mercuric ions and carboxylate groups of the protecting agent. The 1630 cm^{-1} peak does not show any shift in all of the samples. The 1384 cm^{-1} feature was decreasing with an increase in concentration and is completely absent in mercuric citrate. All of the remaining features of citrate were present, which indicated that citrate protection was still present on the nanoparticle.

The SEM image of Ag@citrate treated with 100 ppm solution is shown in Figure S7A (SI). The nanoparticles are aggregated after the treatment. An EDAX spectrum of Ag@citrate (Figure S7B, SI) suggests the presence of all of the possible elements in the reaction mixture, including mercury. Bulk silver did not show Hg(II) uptake, which was confirmed by column studies. The uptake of mercury by silver nanoparticles is confirmed by the elemental maps shown in Figure 2. In the solid state, particles appear as aggregates, as expected. The TEM images of nanoparticles treated with 0.1, 10, and 100 ppm Hg(II) solutions are shown in Figure 2, and their elemental maps and EDAX spectra are shown in Figures S8 and S9 (SI), respectively. In general, the particle size decreases with the extended reaction, as seen from the images. This suggests core etching, and it does not happen at low concentrations, where the particles appear similar to the parent Ag@citrate. At 0.1 ppm, almost no mercury uptake was observed (Figure S8, SI) as evidenced by the EDAX spectrum (Figure S9, SI). This is in agreement with the TEM data. The aggregation of nanoparticles because of the interaction between the nanoparticles and the Hg(II) ions is further confirmed by DLS measurements. The average hydrodynamic diameters observed were 22.8, 38.8, 97.6, and 54.3 nm in pristine Ag@citrate and 0.1, 10, and 100 ppm solutions, respectively, as shown in Figure S10 (SI). A systematic increase in the size and size distribution is seen, although the average size of the 100 ppm sample is lower than that of 50 ppm sample. Thus, although the particles appear smaller in TEM, they exist as aggregates in solution. The ζ potentials of Ag@citrate and 0.1, 10, and 100 ppm solutions were measured to be -26.7 ± 2.6 , -26.9 ± 4.5 , -52.7 ± 9.4 , and -32.9 ± 3.2 mV, respectively. The ζ potential data also support the other observations. In effect, the parent and 0.1 ppm samples are similar in size and charge, but the higher concentration samples are aggregated in solution. Although they have undergone an

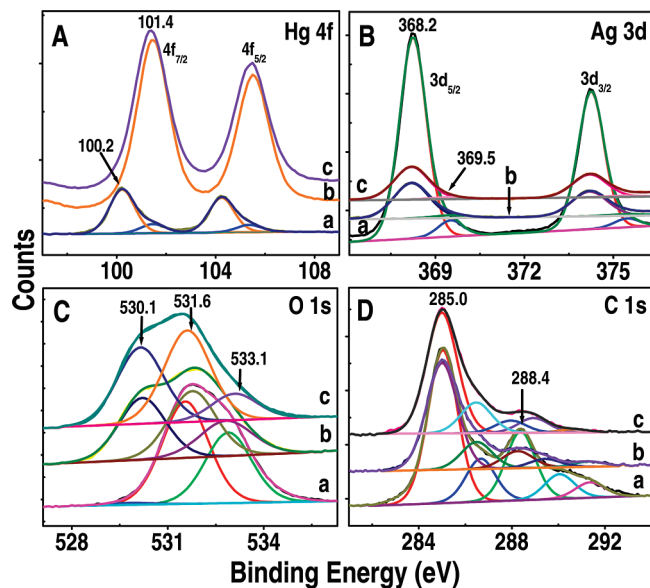


Figure 3. XPS spectra of Ag@citrate residues obtained after treatment with the 10, 50, and 100 ppm of Hg(II) solutions (traces a, b, and c) with Ag@citrate nanoparticles. Hg 4f, Ag 3d, O 1s, and C 1s regions are shown in A–D.

extensive reaction as seen in TEM, the particles are still negatively charged, indicating the presence of the carboxylate protection.

The XPS spectrum of Hg-citrate is shown in Figure S11 (SI). The presence of carbon, mercury, and oxygen is seen in surveying the spectrum in Figure S11A (SI). In Figure S11B (SI) the peak at $101.7 (\pm 0.4)$ eV corresponds to Hg(II) bonded to carboxylate groups. A peak at 533.1 eV corresponds to carboxylate oxygen bonded to Hg(II) (Figure S11C, SI). The C 1s at 288.5 eV is due to carboxylate carbon (Figure S11D, SI). XPS data of the reaction residues are shown in Figure 3. In the 10 ppm reaction, the Hg $4f_{7/2}$ peak (Figure 3A) was observed at 100.2 eV, which is the characteristic binding energy of mercury in the metallic state.³³ This reduction may be due to the electrons donated by the core atoms of the silver nanoparticles. Along with the Hg(0) peak, another peak at 101.4 eV was also observed. This may be due to an intermediate oxidation state: Hg(I) or due to adsorbed Hg(II). It may also be due to the coordination of Hg(II) with the carboxylate groups of the citrate ions as in the case of Hg(II)citrate.³² The XPS peaks, Hg 4f of Hg(I) and Hg(II), are close, and therefore, it is unable to differentiate between the two.³³ Similarly, in the 50 and 100 ppm Hg(II) solutions, also, the peak at 101.4 eV was observed prominently, but the metallic state was not seen. This may be due to the large concentration of Hg(II) ions in the solution. Adsorption or reduction to Hg(I) or complexation³² is dominant instead of reduction to Hg(0) in such a case. The Ag $3d_{5/2}$ peak was seen at 368.2 eV in all three cases, indicating that most parts of the silver nanoparticles are still present in the metallic state (Figure 3B). The presence of another peak in all three cases at 369.5 eV is due to silver atoms bonding with the carboxylate groups of citrate.²⁸ This indicates the presence of protected citrate, even after treatment with mercuric ions. The oxidation of silver was also observed. The Ag $3d_{5/2}$ around $367.5 (\pm 0.2)$ eV is due to oxides of silver. The separation of the oxide peak from the metallic peak is only 0.5 eV, and a clear resolution is difficult.²⁵ In all cases, this oxidation was observed, which is confirmed by O 1s spectra. This may be due to unavoidable oxidation of Ag(0) to Ag_2O .²⁵ It is difficult to differentiate whether it is due to the loss of electrons used for the reduction

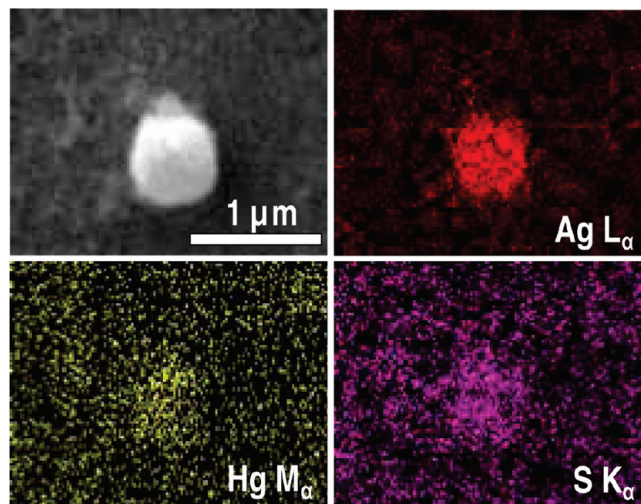


Figure 4. Elemental mapping of Ag@MSA nanoparticle aggregate. The particles were treated with 100 ppm Hg(II) solution.

of mercuric ions or due to aerial oxidation. The peak of O 1s at $530.1 (\pm 0.3)$ eV in Figure 3C is due to oxide. A peak at 531.0 eV may be due to hydroxyl group, and that at $532.6 (\pm 0.3)$ eV is due to the oxygens of carboxylate groups bound to metal ions.²¹ The presence of C 1s peaks at $286.5 (\pm 0.2)$, $288.4 (\pm 0.2)$, and $290.7 (\pm 0.2)$ eV indicate the presence of carboxylate groups in different chemical environments (Figure 3D). Combining the FTIR and XPS data, we can see a systematic increase in the extent of interaction between the monolayers and Hg(II) with an increase in the concentration of the latter.

Treatment of Ag@MSA Nanoparticles with Hg(II). Ag@MSA in 10, 50, and 100 ppm solutions showed absorption at 402, 425, and 420 nm, respectively (Figure S12, SI). These red-shifted values from Ag@MSA absorption (391 nm) correspond to the aggregation of nanoparticles. The IR spectra of the reaction products are shown in Figure S13 (SI). The IR band at 1574 cm^{-1} in Ag@MSA was shifted to 1580 cm^{-1} , in all three reaction mixtures (10, 50, and 100 ppm), which is due to the asymmetric stretching of the $-\text{COO}^-$ group. The similarity of the peak position in all of the samples indicates that the extent of interaction with the carboxyl functionality is essentially the same. The intensity of 1632 cm^{-1} peak decreases, whereas the 1580 cm^{-1} peak increases with an increase in concentration. The remaining features of MSA were similar to Ag@MSA particles, indicating that MSA is still bonded to nanoparticles. The SEM image of 100 ppm solution is shown in Figure S14A (SI), in which aggregated nanoparticles are seen. The EDAX spectrum showed the presence of mercury, silver, and sulfur as the main elements in the sample, as shown in Figure S14B (SI). The elemental mapping of nanoparticles is shown in Figure 4, in which the uptake of mercury was confirmed.

The XPS spectra of the reaction products are shown in Figure 5. In 10 and 50 ppm solutions, the Hg $4f_{7/2}$ peak was seen at $99.9 (\pm 0.3)$ eV, which shows the binding energy corresponding to metallic mercury (Figure 5A).³⁵ This may be due to the reduction of mercuric ions, in which electrons were supplied by the core atoms of the silver nanoparticles. But, this reduction was gradually decreasing with an increase in mercuric ion concentration. Along with the metallic peak, other peaks were also observed. In all three cases (10, 50, and 100 ppm solutions), a prominent peak was seen at 101.3 eV. It may be due to the adsorption of Hg(II) or an intermediate Hg(I) state. The metallic peak was not seen in the 100 ppm case. In 100 ppm solution, the peak at 102.8 eV may be due to the formation of sulfides

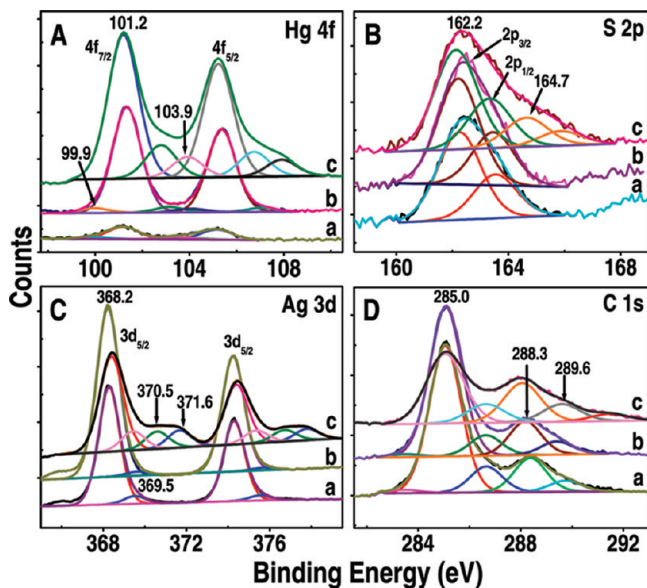


Figure 5. XPS spectra of Ag@MSA residues obtained after treatment with 10, 50, and 100 ppm of Hg(II) solutions (traces a, b, and c) with Ag@MSA nanoparticles. Hg 4f, S 2p, Ag 3d, and C 1s regions are shown in A–D. The metallic peak at 99.9 eV in trace a of part A appears weak, but it can be seen prominently upon enlargement.

with mercuric ions. These sulfides may be disulfides, because in the monosulfide like HgS, the Hg 4f_{7/2} peak is expected at 101.0 eV.³⁶ For the disulfide, mercury should bind to two electronegative sulfur atoms. This is supported by the S 2p_{3/2} peak (Figure 5B). This sulfide formation may be due to the high affinity of heavy metal ions such as Hg, Pb, and Cd toward sulfur. The Hg 4f_{7/2} at 103.1 eV in 50 ppm and 104 eV in 100 ppm are due to the coordination³⁷ of mercuric ions with carboxylic groups of MSA. This aspect will be discussed later.

The S 2p_{3/2} peaks at 162.2 eV in all three cases indicate that the protecting agent was still chemically bonded to the silver nanoparticle surface (thiolates).³⁰ In 10 and 50 ppm cases, the whole of the protecting agent is bonded to the nanoparticle surface, whereas in the 100 ppm case, one more peak of S 2p_{3/2} occurred at 164.7 eV, suggesting that a change happened in the monolayer of the capping agent. This may be due to the formation of sulfides (disulfides).^{36a} The formation of disulfides may be due to the mild oxidants or X-ray induced damage.^{36b} In all three reaction residues, the Ag 3d_{5/2} peaks were seen at 368.2 eV, indicating the presence of silver in the metallic state (Figure 5C). A broad region of Ag 3d_{5/2} around 367.5 (± 0.3) eV corresponds to oxidized silver (Ag₂O and AgOH).^{27,34} But the additional peaks at 370.5 and 371.6 eV can only be seen when the Ag(I) ions combine with electronegative groups like carboxylates. This indicates that silver ions from AgOH or Ag₂O may be interacting with MSA to yield these peaks. The peak at 369.5 eV may be due to the presence of bonded silver atoms to the protecting agent.^{28,29} This coordination is reflected in the high binding energy regions of C 1s and O 1s also. The peaks at 288.3, 289.6, and 291.5 eV are due to carboxylate groups in different chemical environments (Figure 5D). The O 1s at 532.4 eV may be due to oxygens of carboxylate groups linked to the metal ions (Figure S15, SI).²¹ The O 1s at 530.3 eV may be due to oxides of silver, and the peak at 531.3 eV may be due to hydroxides of silver.

Treatment of Ag@citrate Nanoparticles with Hg(I). For the interaction of Hg₂(NO₃)₂ with both Ag@citrate and Ag@MSA nanoparticles, the observations were similar. Because of the low solubility of Hg₂(NO₃)₂, we chose 10, 30, and 50 ppm

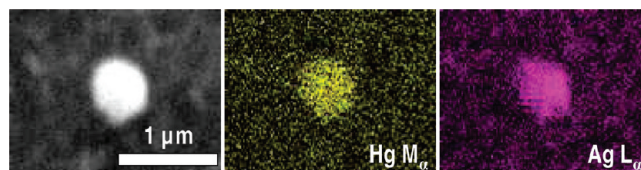


Figure 6. Elemental mapping of Ag@citrate nanoparticles, treated with 50 ppm Hg(I) solution. An aggregated particle is shown.

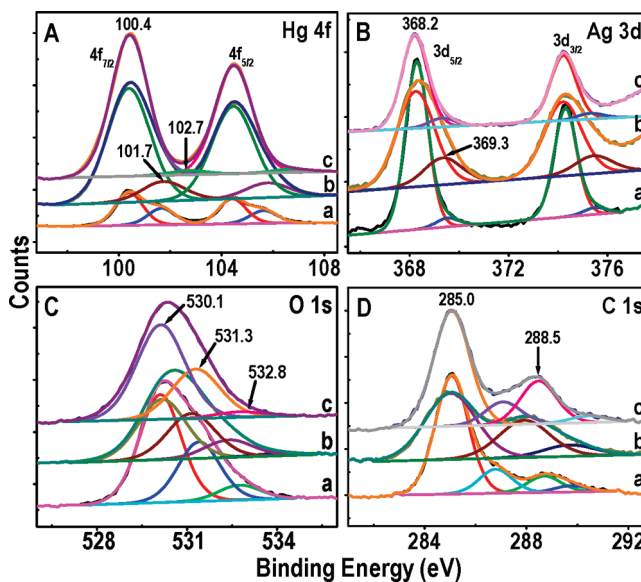


Figure 7. XPS spectra of Ag@citrate residues obtained after treatment with 10, 30, and 50 ppm of Hg(I) solutions (traces a, b, and c) with Ag@citrate nanoparticles. Hg 4f, Ag 3d, O 1s, and C 1s regions are shown in A–D.

concentrations. After treating Ag@citrate nanoparticles with Hg(I) ions, the plasmon band of silver nanoparticles got red-shifted, due to aggregation, as shown in Figure S16A (SI). The IR spectra of the reaction residues exhibit similar features as that of Ag@citrate-Hg(II), as shown in Figure S16B (SI). A peak at 1595 cm⁻¹ in Ag@citrate nanoparticle got shifted to 1585 cm⁻¹ in all three cases (10, 30, and 50 ppm Hg(I)), which may be due to metal–ion interaction with carboxylate groups of citrate. The SEM images were taken for the 50 ppm product in which nanoparticles were aggregated, as shown in Figure S17A (SI). The EDAX spectrum is also shown in Figure S17 (SI). The elemental mapping of nanoparticles is shown in Figure 6, and the uptake of Hg(I) was confirmed.

The XPS data of the reactions of 10, 30, and 50 ppm are shown in Figure 7. The reduction of Hg(I) to Hg(0) with Ag@citrate nanoparticles was confirmed by the presence of a Hg 4f_{7/2} peak at 100.4 eV (Figure 7A), in all three cases (10, 30, and 50 ppm). Along with the metallic peak, in 10 and 30 ppm solutions, a peak of Hg 4f_{7/2} at 101.7 eV and in 50 ppm case a peak at 102.7 eV were also observed. These may be due to the adsorption of Hg(I) ions or may be due to interaction with carboxylate groups of the citrate.³² The peak of Ag 3d_{5/2} was seen at 368.2 eV, which is due to metallic silver (Figure 7B), and 369.3 eV is due to silver atoms bonded to the protecting agent, in all three cases.^{28,29} The O 1s at 530.1 eV may be due to silver oxide,²⁵ 531.3 eV to the hydroxyl group in citrate, and 532.8 eV to oxygens of carboxylates bonded²¹ to metal ions (Figure 7C). The presence of carboxylate groups in different chemical environments was confirmed by the peaks at 288.5 and 290.1 eV (Figure 7D).

Treatment of Ag@MSA Nanoparticles with Hg(I). We have studied the interaction of Ag@MSA nanoparticles with

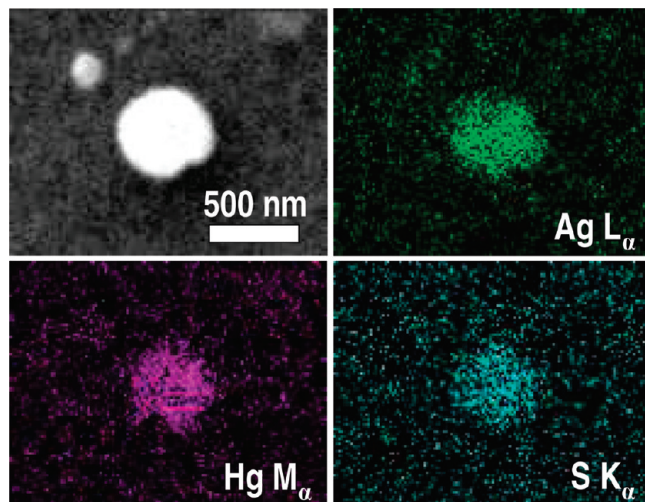


Figure 8. Elemental mapping of Ag@MSA nanoparticles, after treatment with 50 ppm Hg(I) solution. An aggregate of nanoparticle is imaged.

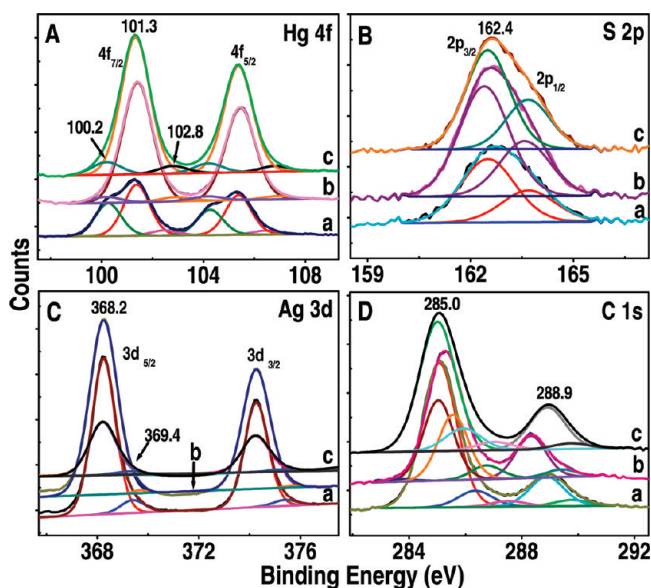


Figure 9. XPS spectra of Ag@MSA residues obtained after treatment with 10, 30, and 50 ppm of Hg(I) solutions (traces a, b, and c) with Ag@MSA nanoparticles. Hg 4f, S 2p, Ag 3d, and C 1s regions are shown in A–D.

Hg(I) ions. The UV–vis and IR spectra are shown in Figure S18 parts A and B (SI), respectively. The IR spectra of the reaction mixtures showed the same features of Ag@MSA nanoparticles, suggesting the presence of a capping agent after the addition of Hg(I) ions. The IR band at 1572 cm^{-1} in Ag@MSA got shifted to 1582 cm^{-1} , indicating the chemical interaction of carboxylic groups of MSA with the metal ions. An SEM image of 50 ppm solution is shown in Figure S19A (SI), in which the aggregation of nanoparticles was observed. EDAX data are also shown in Figure S19 (SI). Aggregation is reflected in the UV–vis data, where the silver plasmon band was shifted to a higher wavelength. The elemental mapping of nanoparticles is shown in Figure 8, which confirms the uptake of mercury.

XPS data of Ag@MSA–Hg(I) reaction products are shown in Figure 9. Hg(I) was reduced to metallic Hg at the core of the nanoparticle, followed by adsorption of Hg(I), along with interaction with the protecting agent (Figure 9A). The fraction of Hg(I) getting reduced decreases with the increase in Hg(I)

concentration. A metallic mercury peak was seen at 100.2 eV .³³ A peak at $102.5 (\pm 0.3)\text{ eV}$ may be due to the interaction of Hg(I) with carboxylate groups of MSA. The peak of S $2p_{3/2}$ was observed at $162.5 (\pm 0.2)\text{ eV}$ (Figure 9B), indicating that the monolayer of the protecting agent on silver nanoparticles was undisturbed.³⁰ Still, the protecting agent is chemically bonded to the nanoparticle surface through sulfur. Ag $3d_{5/2}$ at 368.2 eV indicates the presence of silver in the metallic state (Figure 9C). A peak Ag $3d_{5/2}$ at 369.4 eV may be due to silver atoms bonded to the protecting agent.^{28,29} The presence of $286.3 (\pm 0.2)$ and $288.4 (\pm 0.3)\text{ eV}$ peaks confirms the presence of carboxylate groups in different chemical environments (Figure 9D). The O 1s spectra of the above reaction residues are shown in Figure S20 (SI). The peak of O 1s at $530.9 (\pm 0.3)\text{ eV}$ corresponds to oxide,²⁵ and that at $533.6 (\pm 0.3)\text{ eV}$ corresponds to carboxylate oxygens bonded to metal ions.

Treatment of Ag@citrate and Ag@MSA Nanoparticles with Pb(II) and Cd(II). Interaction of cadmium acetate and lead acetate with both Ag@citrate and Ag@MSA nanoparticles were studied similarly. The UV–vis, IR, and SEM data of these reaction mixtures are shown in Figures S21–S28 (SI). After treating both nanoparticles with Cd(II) and Pb(II) ions, the aggregation of the nanoparticles was noticed in SEM images, which was also supported by the red shift in the absorption bands. The interaction of Cd(II) and Pb(II) ions with carboxylate groups of the capping agents (citrate and MSA) is supported by the shift of carboxylate groups in the IR spectra (SI). XPS data alone are shown here. These metal ions were not undergoing reduction. The reason could be the more negative reduction potential of lead and cadmium than silver.⁹ But, they were showing adsorption and chemical interactions with the protecting agent on the nanoparticle surface. After adsorption, they are converted to oxides in the case of Ag@citrate and sulfides³⁸ in the case of Ag@MSA. These conversions were investigated by XPS. The XPS peaks at a higher binding energy region than the metallic state indicates the interaction between the metal ions and the carboxylate groups of MSA and citrate.

In an Ag@citrate–Cd(II) interaction, similar observations are made in all three concentrations. Cd $3d_{5/2}$ at $405.6 (\pm 0.4)\text{ eV}$ corresponds to CdO,³⁹ and that at 407.4 eV is due to interaction with carboxylate groups of citrate (Figure 10A). The presence of metallic silver^{27,28} (368.2 eV) and silver bonded to the protecting agent^{28,29} (369.3 eV) are all seen in Figure 10B. The oxide²⁵ oxygens shown at 530.2 , 531.8 , and 533.9 eV are due to carboxylate oxygens bonded to metal ions (Figure 10C). The presence of C 1s at 288.2 and 289.6 eV corresponds to carboxylate carbons (Figure 10D).

In an Ag@citrate–Pb(II) interaction, the peak of Pb $4f_{7/2}$ at 138.6 eV can be assigned to PbO,⁴⁰ and the high binding energy peak at 141.3 eV may be due to its interaction with carboxylic groups of citrate (Figure 11A). The presence of metallic silver^{27,28} (Ag $3d_{5/2}$ at 368.2 eV) and silver bonded to the protecting agent^{28,29} (369.2 eV) can be seen in Figure 11B. The oxide²⁵ oxygen was seen at 530.3 eV , and that at 532.9 eV may be due to carboxylate oxygens bonded to metal ions (Figure 11C). The carboxylate carbons in different chemical environments were observed at 288.3 , 290.2 , and 291.7 eV (Figure 11D).

In Ag@MSA–Cd(II) interaction, the peak of Cd $3d_{5/2}$ at 405.5 eV can be attributed to CdO or CdS,⁴¹ and that at $407.2 (\pm 0.2)\text{ eV}$ is due to the interaction with carboxylate groups of MSA (Figure 12A). The peak of S $2p_{3/2}$ at 162.2 eV is assigned to bound sulfur to the nanoparticles or sulfide of cadmium,⁴¹ and that at $164.0 (\pm 0.3)\text{ eV}$ corresponds to disulfides.³⁶ The

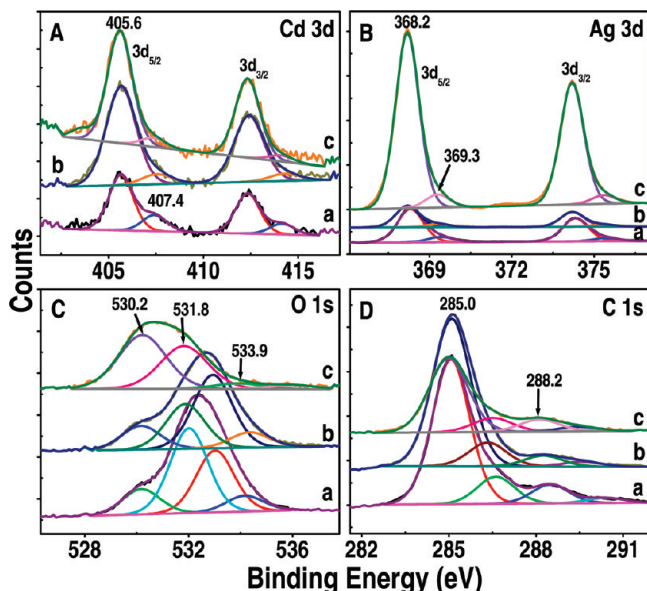


Figure 10. XPS spectra of Ag@citrate residues obtained after treatment with 10, 50, and 100 ppm of Cd(II) solutions (traces a, b, and c) with Ag@citrate nanoparticles. Cd 3d, Ag 3d, O 1s, and C 1s regions are shown in A–D.

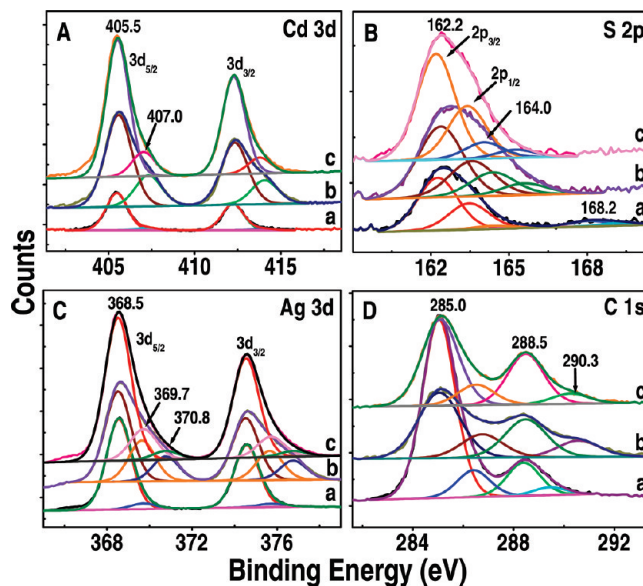


Figure 12. XPS spectra of Ag@MSA residues obtained after treatment with 10, 50, and 100 ppm of Cd(II) solutions (traces a, b, and c) with Ag@MSA nanoparticles. Cd 3d, S 2p, Ag 3d, and C 1s regions are shown in A–D.

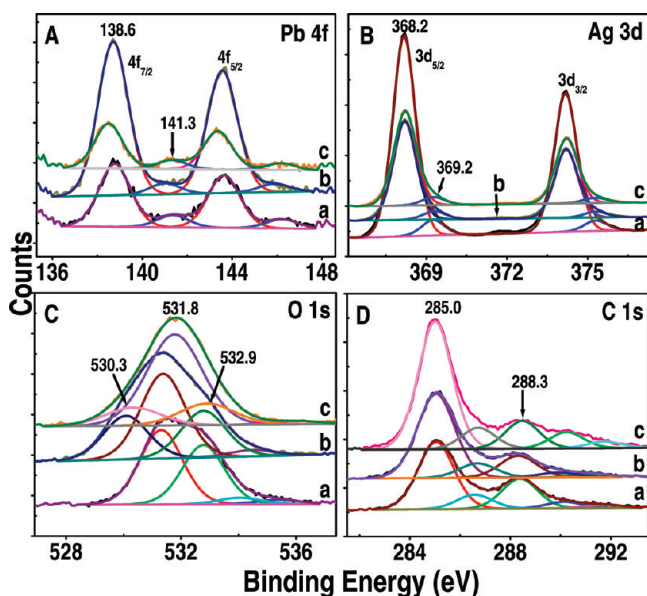


Figure 11. XPS spectra of Ag@citrate residues obtained after treatment with 10, 50, and 100 ppm of Pb(II) solutions (traces a, b, and c) with Ag@citrate nanoparticles. Pb 4f, Ag 3d, O 1s, and C 1s regions are shown in A–D.

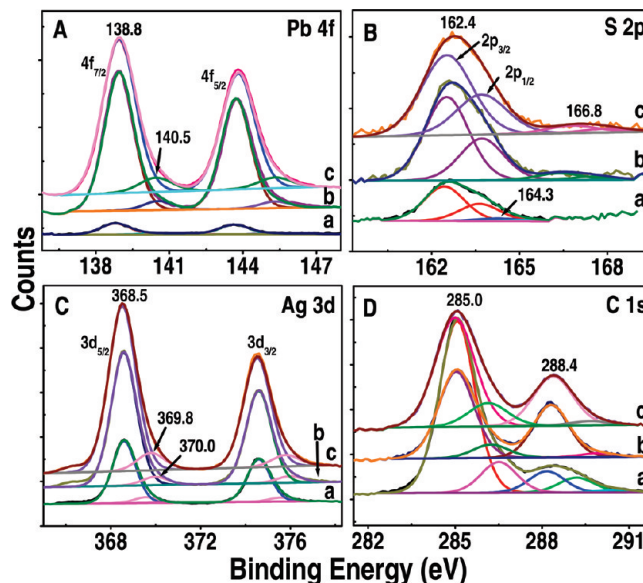


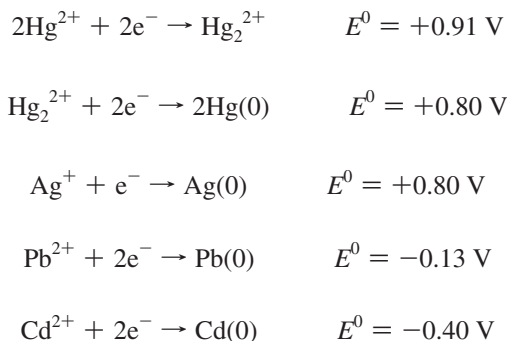
Figure 13. XPS spectra of Ag@MSA residues obtained after treatment with 10, 50, and 100 ppm of Pb(II) solutions (traces a, b, and c) with Ag@MSA nanoparticles. Pb 4f, S 2p, Ag 3d, and C 1s regions are shown in A–D.

formation of oxidized sulfur⁴¹ (sulfate) at 168.2 eV was observed in the 10 ppm reaction (Figure 12B). This may be due to aerial oxidation, while we kept the samples for drying prior to analysis or X-ray induced damage.³¹ The presence of metallic silver^{27,28} (Ag 3d_{5/2}) at 368.2 eV and silver bonded to the protecting agent^{28,29} at 369.3 eV can be seen in Figure 12C. The C 1s peaks at 288.5 and 290.3 eV correspond to carboxylate carbons in different chemical environments (Figure 12D). The O 1s spectra are shown in Figure S29 (SI). The peak at 529.7 (± 0.3) eV corresponds to oxide,²⁵ and those at 532.6 and 534.0 eV may be due to carboxylate oxygens bonded to metal ions.

In the case of Ag@MSA interaction with Pb(II), the peaks of Pb 4f_{7/2} at 138.8 eV are due to lead sulfides,⁴² and the other high binding energy peak at 140.4 (± 0.2) eV may be due to the interaction of carboxylic groups of MSA with Pb(II) ions

(Figure 13A). In Figure 13B, the peak at 162.4 eV is assigned to bound sulfur,³⁰ and in 10 ppm reaction, S 2p_{3/2} at 164.3 eV may be due to disulfides.³⁶ The peaks at 166.6 (± 0.2) eV are due to sulfite formation. The metallic silver^{27,28} (Ag 3d_{5/2}) at 368.3 (± 0.2) eV and silver bonded to the protecting agent^{28,29} (369.5 (± 0.3) eV) are also seen in Figure 13C. The C 1s peaks at 288.4 and 289.7 eV correspond to the carboxylate groups in different chemical environments (Figure 13D). The O 1s peak is shown in Figure S30 (SI). The peak at 529.6 (± 0.4) eV is due to oxide,²⁵ and that at 533.0 (± 0.4) eV is due to oxygens of carboxylate bonded to metal ions.

Electrochemical Reason for the Reduction of Metal Ions. The standard reduction potentials of Hg(II), Hg(I), Pb(II), and Cd(II) are as follows:



The cell emf (electromotive force) for the reaction, $n\text{Ag}(0) + \text{M}^{n+} \rightarrow n\text{Ag}^+ + \text{M}(0)$ (1) or $x\text{Ag}(0) + \text{M}^{n+} \rightarrow x\text{Ag}^+ + \text{M}^{(n-x)+}$ (2), is positive only for reaction 2 with Hg(II). But, this emf is not largely positive, so the reduction is not highly favored. The cell emf is zero for Hg(I) for reaction 1; it should be a reversible reaction. Since Ag(0) is in the nanoscale, it can get oxidized easily, facilitating the reduction of metal ions. For Cd(II)/Ag(0) and Pb(II)/Ag(0) systems, the cell emf is negative for reaction 1. Silver cannot undergo oxidation, giving electrons to Pb(II) and Cd(II), which is further supported by XPS. It is possible that these metal ions adsorb on the nanoparticle surfaces, and this is confirmed by EDAX and XPS. Besides these reactions with the metal cores, there are also reactions with the monolayers.

On the basis of our findings, we propose the following scheme. When different metal ions at varying concentrations are treated with Ag@citrate nanoparticles, depending on the cell emf of the reaction system, different possible interactions occur. In Ag@citrate nanoparticles, the protection is by charge stabilization through carboxylate groups of citrate. At lower metal ion concentrations, the affinity of metal ions to the core decides the interaction. Because of that, Hg(II) and Hg(I) reduction occur predominantly. Adsorption on the monolayer with both the head and tail groups will increase with an increase in metal ion concentration. In Ag@citrate/metal ion systems, there is a possibility for the interaction of metal ions with the carboxylate groups. The XPS peaks in the high binding energy regions of metal ions rather than in their metallic state can only be explained by interaction with electronegative groups like carboxylate groups.

In Ag@MSA/metal ion systems, reduction happens for mercuric and mercurous ions. Adsorption and chemical interaction occurred in all of the metal ions we studied. The heavy metal ions have a strong affinity toward sulfur. As the thiolate group behaves as soft acid, it would form stable compounds with soft bases³⁸ such as mercuric, cadmium, and lead ions. This leads to sulfides/disulfides. In Ag@MSA nanoparticles, the carboxylate groups of MSA are projecting outward. So the metal ions can directly interact with the carboxylate groups. This kind of ligand coordination is supported by the literature.^{32,37,43} The interaction of silver ions from oxide (Ag₂O) with carboxylate groups of the capping agents was also observed. In Figure 14, we illustrate the situation schematically.

Additional interaction of metal ions with Ag@MSA suggests its larger uptake capacity. This aspect is under investigation.

Conclusions

Ag@citrate and Ag@MSA nanoparticles were treated with heavy metal ions, and their interaction with the metal core and the capping agents was investigated. At lower concentrations of metal ions, they interact with the metal core. At sufficiently higher concentrations of metal ions, there is a chance for metal

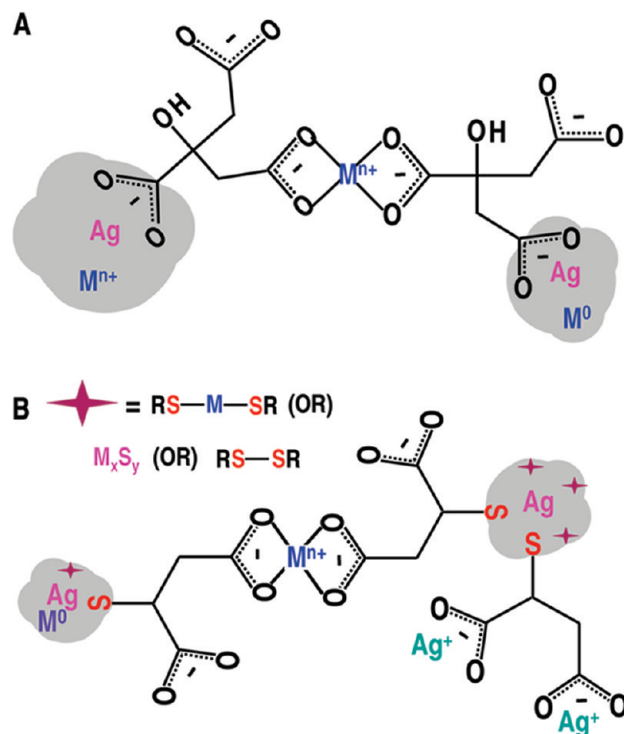


Figure 14. Schematic representation of the interaction of heavy metal ions (Hg(I), Hg(II), Pb(II), and Cd(II)) with Ag@citrate (A) and Ag@MSA (B) nanoparticles. The particles are nonspherical. Ag@MSA particles are much smaller than those of Ag@citrate. In Ag@citrate, metal ion reduction at the nanoparticle surface as well as coordination with the carboxylate groups occurs. For Ag@MSA, besides these, a metal sulfide/disulfide is also formed. Metal sulfide (M_xS_y) or other sulfur species are shown by the star symbol. In part B, R refers to the alkyl moiety of MSA.

ions to interact with the capping agent. Hg(I) and Hg(II) were reduced to Hg(0) first, followed by adsorption and coordination with the carboxylate groups of the protecting agents (citrate and MSA). The sulfur-containing species formed are physisorbed on the nanoparticle surface or dimerized to form disulfide. In the case of Pb(II), the formation of sulfites was observed. This may be due to aerial oxidation of physisorbed sulfur species or due to X-ray induced damage. In all cases, the monolayers are retained on the nanoparticle surfaces. The use of noble metal nanoparticles in heavy metal ion scavenging from water is clear from this study.

Acknowledgment. We thank the Department of Science and Technology, Government of India, for constantly supporting our research program on nanomaterials. We thank Dr. Balachandran Unni Nair and Mr. M. Nidhin, CLRI, Chennai, for the DLS measurements. M.S.B. thanks the CSIR for a research fellowship.

Supporting Information Available: UV-vis and IR spectra, TEM and SEM images, and EDAX of Ag@citrate and Ag@MSA, before and after treatment with different concentrations of Hg(II), Hg(I), Cd(II), and Pb(II). This material is available free of charge via the Internet at <http://pubs.acs.org>.

References and Notes

- (1) Nolan, E. M.; Lippard, S. J. *Chem. Rev.* **2008**, *108*, 3443–3480.
- (2) Chillemi, G.; Mancini, G.; Sanna, N.; Barone, V.; Longa, S. D.; Benfatto, M.; Pavel, N. V.; D'Angelo, P. *J. Am. Chem. Soc.* **2007**, *129*, 5430–5436.

- (3) Das, S. K.; Das, A. R.; Guha, A. K. *Environ. Sci. Technol.* **2007**, *41*, 8281–8287.
- (4) Lee, J. S.; Han, M. S.; Mirkin, C. A. *Angew. Chem., Int. Ed.* **2007**, *46*, 4093–4096.
- (5) *Mercury Update: Impact of Fish Advisories*, EPA Fact Sheet EPA-823-F-01-011; EPA, Office of Water: Washington, DC, 2001.
- (6) (a) Li, P.; Feng, X. B.; Qiu, G. L.; Shang, L. H.; Li, Z. G. *J. Hazard. Mater.* **2009**, *168*, 591–601. (b) Yudovich, Y. E.; Ketris, M. P. *Int. J. Coal Geol.* **2005**, *62*, 107–134.
- (7) (a) Lacerda, L. D. *Water, Air, Soil Pollut.* **1997**, *97*, 209–221. (b) Streets, D. G.; Zhang, Q.; Wu, Y. *Environ. Sci. Technol.* **2009**, *43*, 2983–2988.
- (8) Lisha, K. P.; Anshup; Pradeep, T. *Gold Bull. (Geneva)* **2009**, *42*, 144–152.
- (9) (a) Li, X. Q.; Zhang, W. *J. Phys. Chem. C* **2007**, *111*, 6939–6946. (b) Li, X. Q.; Zhang, W. *Langmuir* **2006**, *22*, 4638–4642. (c) Sherman, M. P.; Darab, J. G.; Mallouk, T. E. *Environ. Sci. Technol.* **2000**, *34*, 2564–2569.
- (10) Rex, M.; Hernandez, F. E.; Campiglia, A. D. *Anal. Chem.* **2006**, *78*, 445–451.
- (11) Pradeep, T.; Anshup. *Thin Solid Films* **2009**, *517*, 6441–6478.
- (12) Nair, S.; Pradeep, T. *J. Nanosci. Nanotechnol.* **2007**, *7*, 1–7.
- (13) Jain, P.; Pradeep, T. *Biotechnol. Bioeng.* **2005**, *90*, 59–63.
- (14) Jayaraman, K. *Chem. World* **2007**, *4*, 15–15.
- (15) Kamat, P. V.; Flumiani, M.; Hartland, G. V. *J. Phys. Chem. B* **1998**, *102*, 3123–3128.
- (16) Mrudula, K. V.; Udaya Bhaskara Rao, T.; Pradeep, T. *J. Mater. Chem.* **2009**, *19*, 4335–4342.
- (17) Choia, S. H.; Leeb, S. H.; Hwanga, Y. M.; Leea, K. P.; Kang, H. D. *Radiat. Phys. Chem.* **2003**, *67*, 517–521.
- (18) Kimura, K.; Yao, H.; Sato, S. *Synth. React. Inorg. Met.-Org. Chem.* **2006**, *36*, 237–264.
- (19) Nair, S.; Kimura, K. *Phys. Chem. Chem. Phys.* **2009**, *11*, 9346–9350.
- (20) Bovi Mitre, M. G.; Wierna, N. R.; Wagner, C. C.; Baran, E. J. *Biol. Trace Elem. Res.* **2000**, *76*, 183–190.
- (21) Tselesh, A. S. *Thin Solid Films* **2008**, *516*, 6253–6260.
- (22) Chen, S.; Kimura, K. *Langmuir* **1999**, *15*, 1075–1082.
- (23) Zhang, F. X.; Guan, N. J.; Li, Y. Z.; Zhang, X.; Chen, J. X.; Zeng, H. S. *Langmuir* **2003**, *19*, 8230–8234.
- (24) Wang, C.; Yifeng, E.; Fan, L.; Yang, S.; Li, Y. *J. Mater. Chem.* **2009**, *19*, 3841–3846.
- (25) (a) Dong, J.; Xu, Z.; Kuznicki, S. M. *Adv. Funct. Mater.* **2009**, *19*, 1268–1275. (b) Janardhanan, R.; Karuppaiah, M.; Hebalkar, N.; Narsinga Rao, T. *Polyhedron* **2009**, *28*, 2522–2530.
- (26) Yoshimoto, K.; Nozawa, M.; Matsumoto, S.; Echigo, T.; Nemoto, S.; Hatta, T.; Nagasaki, Y. *Langmuir* **2009**, *25*, 12243–12249.
- (27) Zhang, H.; Wang, G.; Chen, D.; Lv, X.; Li, J. *Chem. Mater.* **2008**, *20*, 6543–6549.
- (28) Mackova, A.; Svoricik, V.; Sajdl, P.; Stryhal, Z.; Pavlik, J.; Malinsky, P.; Slouf, M. *Vacuum* **2008**, *82*, 307–310.
- (29) Biniak, S.; Pakula, M.; Swiatkowski, A. *J. Appl. Electrochem.* **1999**, *29*, 481–487.
- (30) Gonella, G.; Cavalleri, O.; Terreni, S.; Cvetko, D.; Floreano, L.; Morgante, A.; Canepa, M.; Rolandi, R. *Surf. Sci.* **2004**, *566–568*, 638–643.
- (31) Sandhyarani, N.; Pradeep, T. *Int. Rev. Phys. Chem.* **2003**, *22*, 221–262.
- (32) Yoosaf, K.; Ipe, B. I.; Suresh, C. H.; Thomas, K. G. *J. Phys. Chem. C* **2007**, *111*, 12839–12847.
- (33) Wang, J.; Deng, B.; Chen, H.; Wang, X.; Zheng, J. *Environ. Sci. Technol.* **2009**, *43*, 5223–5228.
- (34) Morrish, R.; Muscat, A. *J. Chem. Mater.* **2009**, *21*, 3865–3870.
- (35) Genin, F.; Alnot, M.; Ehrhardt, J. *J. Appl. Surf. Sci.* **2001**, *173*, 44–53.
- (36) (a) Castner, D. G.; Hinds, K.; Grainger, D. W. *Langmuir* **1996**, *12*, 5083–5086. (b) Esplandiu, M. J.; Noeske, P. L. M. *Appl. Surf. Sci.* **2002**, *199*, 166–182.
- (37) Murray, R. W. *Chem. Rev.* **2008**, *108*, 2688–2720.
- (38) Yavuz, E.; Barim, G.; Senkal, B. F. *J. Appl. Polym. Sci.* **2009**, *114*, 1879–1883.
- (39) Gulino, A.; Castelli, F.; Dapporto, P.; Rossi, P.; Fragala, I. *Chem. Mater.* **2002**, *14*, 704–709.
- (40) Veluchamy, P.; Minoura, H. *Appl. Surf. Sci.* **1998**, *126*, 241–245.
- (41) Nakanishi, T.; Ohtani, B.; Uosaki, K. *J. Phys. Chem. B* **1998**, *102*, 1571–1577.
- (42) Godocikova, E.; Bastl, Z.; Spirovova, I.; Balaz, P. *J. Mater. Sci.* **2004**, *39*, 3025–3029.
- (43) (a) Liu, X. W.; Hu, Q.; Fang, Z.; Zhang, X.; Zhang, B. *Langmuir* **2009**, *25*, 3–8. (b) Hasan, S.; Krishnaiah, A.; Ghosh, T. K.; Viswanath, D. S. *Ind. Eng. Chem. Res.* **2006**, *45*, 5066–5077. (c) Jhansi Rani, K.; Arbneshi, T.; Khan, S. A.; Neely, A.; Candice, P.; Varisli, B.; Washington, M.; McAfee, S.; Robinson, B.; Banerjee, J.; Singh, A. K.; Senapati, D.; Ray, P. C. *Angew. Chem., Int. Ed.* **2009**, *48*, 1–5. (d) Lu, Q. F.; Huang, M. R.; Li, X. G. *Chem.—Eur. J.* **2007**, *13*, 6009–6018. (e) Li, X. G.; Feng, H.; Huang, M. R. *Chem.—Eur. J.* **2009**, *15*, 4573–581. (f) Macdonald, J. E.; Veinot, J. G. C. *Langmuir* **2008**, *24*, 7169–7177. (g) Sendroiu, I. U.; Schiffrin, D. J.; Abad, J. M. *J. Phys. Chem. C* **2008**, *112*, 10100–10107. (h) Quirarte-Escalante, C. A.; Soto, V.; Cruz, W. D. L.; Porras, G. R.; Manriquez, R.; Gomez-Salazar, S. *Chem. Mater.* **2009**, *21*, 1439–1450. (i) Jiang, P.; Liu, Z. F.; Cai, S. M. *Langmuir* **2002**, *18*, 4495–4499. (j) Liang, X.; Xu, Y.; Sun, G.; Wang, L.; Sun, Y.; Qin, X. *Colloids Surf., A* **2009**, *349*, 61–68.

JP101988H